Experimental Entanglement Redistribution under Decoherence Channels

G. H. Aguilar,[*] A. Valdés-Hernández, L. Davidovich, S. P. Walborn, and P. H. Souto Ribeiro

Instituto de Física, Universidade Federal do Rio de Janeiro, CP 68528, 21941-972, Rio de Janeiro, Rio de Janeiro, Brazil
(Received 21 July 2014; published 9 December 2014)

When an initially entangled pair of qubits undergoes local decoherence processes, there are a number of ways in which the original entanglement can spread throughout the multipartite system consisting of the two qubits and their environments. Here, we report theoretical and experimental results regarding the dynamics of the distribution of entanglement in this system. The experiment employs an all optical setup in which the qubits are encoded in the polarization degrees of freedom of two photons, and each local decoherence channel is implemented with an interferometer that couples the polarization to the path of each photon, which acts as an environment. We monitor the dynamics and distribution of entanglement and observe the transition from bipartite to multipartite entanglement and back, and show how these transitions are intimately related to the sudden death and sudden birth of entanglement. The multipartite entanglement is further analyzed in terms of three- and four-partite entanglement contributions, and genuine four-qubit entanglement is observed at some points of the evolution.

Introduction.—In one of his landmark papers, Schrödinger characterized entanglement in terms closely related to the modern notion of information [1]. According to him, for an entangled system, "best possible knowledge of a whole does not include best possible knowledge of its parts." In the same vein, decoherence processes can be attributed to the loss of information of a quantum system to the environment with which it gets entangled [2]. For a composite system in an entangled state, the initial entanglement, or "information of the whole," can be distributed throughout the system and environment in a number of ways. Depending on the initial state and on the specific interaction with the environment, the redistribution of the entanglement can give rise to phenomena like the entanglement sudden death (ESD) [3,4] and entanglement sudden birth (ESB) [5]. In this Letter, we address the question of what happens with the entanglement in the interval between ESD and ESB.

For an initial bipartite entangled state where one subsystem interacts with the environment, genuine tripartite entanglement may arise in the form of a Greenberger-Horn-Zeilinger [6] or W type [7] of state, including the environmental degrees of freedom [8,9]. Here, we experimentally study two entangled qubits, each one coupled to its local environment. This configuration gives rise to a much richer dynamics, as compared to the tripartite case [8,9], allowing for the detailed study of the ESD and ESB processes and the emergence of genuine four-partite entanglement. The qubits are encoded in the polarizations of two photons, while the decoherence is implemented by optically coupling the polarization to the spatial mode, which plays the role of the environment. Performing quantum state tomography of the complete four-partite system, we analyze the entanglement as a function of the amount of decoherence applied to the system. We

observe both ESD and ESB, and the redistribution of the entanglement from bipartite to tri- and four-partite forms. We also present a theory based on monogamy relations that provides appropriate multipartite entanglement quantifiers.

Monogamy inequalities and residual entanglement.— The monogamy inequality in N-qubit systems reads [10]

$$C^2_{i|j_1,j_2,\ldots,j_{N-1}} \geq C^2_{ij_1} + C^2_{ij_2} + \cdots + C^2_{ij_{N-1}}, \quad (1)$$

where the tangle $C^2_{A|B}$ measures the bipartite entanglement between A and B. If A and B are sets of qubits, then $C^2_{A|B} = \inf_{\{|\phi_l\rangle\langle\phi_l|,p_l\}} \sum_l 2p_l[1 - \mathrm{tr}(\rho^l_A)^2]$, where $\rho^l_A = \mathrm{tr}_B(|\phi_l\rangle\langle\phi_l|)$, and the pure states $|\phi_l\rangle$ are the possible decompositions of ρ_{AB} as $\sum_l p_l|\phi_l\rangle\langle\phi_l|$. If A and B represent single qubits ($A = i$, $B = j$), $C_{A|B}$ is the concurrence [11]

$$C_{ij} = \max\{0, \Gamma\}, \quad (2)$$

where $\Gamma = \sqrt{\lambda_1} - \sqrt{\lambda_2} - \sqrt{\lambda_3} - \sqrt{\lambda_4}$ and the λ_i's are the eigenvalues (in decreasing order) of $\rho_{ij}(\sigma_y \otimes \sigma_y)\rho^*_{ij}(\sigma_y \otimes \sigma_y)$. In addition, for $2N$-qubit systems and partitions $2:2N-2$, it was shown that [12]

$$C^2_{ii'|j_1,j'_1,\ldots,j_{N-1},j'_{N-1}} \geq \sum_{m=1}^{N-1} C^2_{ij_m} + C^2_{ij'_m} + C^2_{i'j_m} + C^2_{i'j'_m}, \quad (3)$$

whenever the reduced density matrix $\rho_{ii'}$ is a rank-two matrix.

We now analyze the monogamy relations in a four-qubit system composed of two open systems S_1 and S_2 and their respective environments E_1 and E_2. We assume that the initial state is

$$|\Psi(0)\rangle_{S_1 S_2 E_1 E_2} = |\psi(0)\rangle_{S_1 S_2}|0\rangle_{E_1}|0\rangle_{E_1}, \quad (4)$$

with $|\psi(0)\rangle$ an entangled state, and that the evolution has the form

$$|\Psi(t)\rangle = U_{S_2 E_2}(t) U_{S_1 E_1}(t) |\Psi(0)\rangle. \qquad (5)$$

With these assumptions, direct calculation shows that $\rho_{S_1 E_1}(t)$ and $\rho_{S_2 E_2}(t)$ are rank-two matrices during the whole evolution; we thus apply Eq. (3) and write the (positive) residual entanglement for the bipartition $S_1 E_1 | S_2 E_2$ as [12]

$$R_{S_1 E_1 | S_2 E_2} \equiv C^2_{S_1 E_1 | S_2 E_2} - C^2_{S_2 E_1} - C^2_{S_1 E_2} - C^2_{S_1 S_2} - C^2_{E_1 E_2}. \qquad (6)$$

Equation (1) gives the residual entanglement for the most unbalanced bipartition

$$R_i \equiv C^2_{i|jkl} - C^2_{ij} - C^2_{ik} - C^2_{il}, \qquad (7)$$

where $i, j, k, l = S_1, S_2, E_1$, and E_2. The residual entanglements encode multipartite (rather than bipartite) entanglement. In particular, for a pure three-qubit state, R_i becomes independent of i and coincides with the three-tangle [13]:

$$\tau_{ijk} = C^2_{i|jk} - C^2_{ij} - C^2_{ik}. \qquad (8)$$

Since Eq. (5) involves local unitary transformations, the entanglement between systems $(S_1 E_1)$ and $(S_2 E_2)$ remains constant; thus, $C^2_{S_1 E_1 | S_2 E_2}$ is conserved and equals the initial entanglement $\mathcal{E}_0^2 \equiv C^2_{S_1 S_2}(0)$.

Experimental setup.—The experimental setup is shown in Fig. 1. The system qubits are encoded in the polarization of two photons, produced with type-I spontaneous parametric down-conversion [14]. The environment is represented by the spatial mode (path) of each photon, initially in the state $|0\rangle_E$. Ideally, the initial two-photon state is

$$|\Psi\rangle = (\alpha |0\rangle_{S_1} |0\rangle_{S_2} + \beta |1\rangle_{S_1} |1\rangle_{S_2}) |0\rangle_{E_1} |0\rangle_{E_2}, \qquad (9)$$

where $|0\rangle_S$ and $|1\rangle_S$ represent the horizontal and vertical polarizations of the photons, respectively. Each photon is directed to optical interferometers that implement a unitary transformation modeling the interaction between the polarization S_i and the spatial mode E_i. A second interferometer, wave plates, and a polarizing beam splitter (PBS) are used to perform full state tomography on the polarization and path degrees of freedom of each photon. We briefly summarize the role of each interferometer, as complete details are given in Refs. [8,9].

The interferometers have calcite beam displacers [BDs, modified beam displacers (MBDs)] to separate horizontal and vertical polarization components. A half wave plate (HWP), with rotation angle θ_p, controls the amount of decoherence. As θ_p varies, the spatial mode one populates according to the map:

$$|0\rangle_S |0\rangle_E \rightarrow |0\rangle_S |0\rangle_E,$$
$$|1\rangle_S |0\rangle_E \rightarrow \sqrt{1-p}|1\rangle_S |0\rangle_E + \sqrt{p}|0\rangle_S |1\rangle_E, \qquad (10)$$
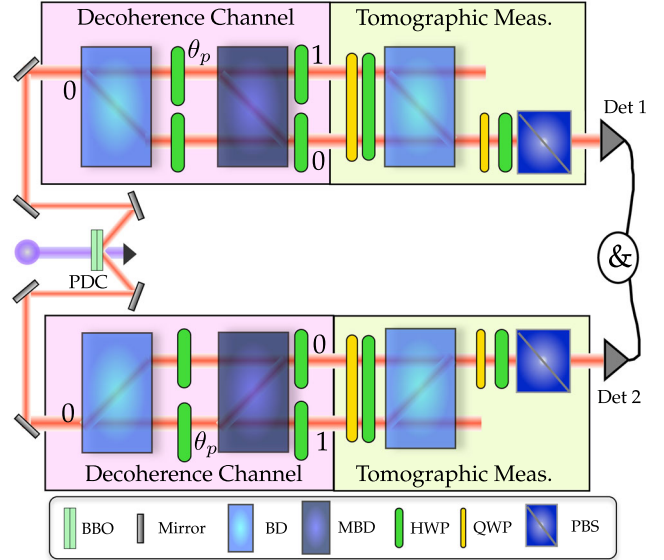

FIG. 1 (color online).   Experimental setup: An ultraviolet laser pumps a nonlinear BBO crystal, and two photons are produced via parametric down-conversion. Both photons are directed to separated nested interferometers. The first interferometers (light red rectangles) have a BD and a MBD. These implement the decoherence channels, as in Refs. [8,9]. The optical elements in the light green rectangles serve to perform tomographic measurements on the polarization and path degrees of freedom simultaneously.

where $p = \sin^2(2\theta_p)$. This transformation corresponds to the amplitude damping channel when the environments are traced out. The second interferometer and the polarization optics shown in the light green rectangles of Fig. 1 serve to perform complete tomography of the polarization and spatial mode using 256 different settings of the HWPs and quarter-wave plates (QWPs) [8,9,15]. That is, we perform complete four-qubit tomography, allowing us to reconstruct the total four-partite state and to completely analyze the evolution of entanglement as p varies.

Distribution of entanglement.—In order to analyze the ESD, the ESB, and the entanglement redistribution, we create photons in the state (9) with $\alpha \simeq \sqrt{1/7}$ and $\beta \simeq \sqrt{6/7}$, with purity 0.82 and fidelity 0.9. Both photons are sent to the interferometers, which implement amplitude damping channels as in Eq. (10). The parameters p_i are varied so that $p_1 = p_2 = p$. The evolved state is

$$|\Psi(p)\rangle_{S_1 S_2 E_1 E_2} = \frac{1}{\sqrt{7}} |0000\rangle + \sqrt{\frac{6}{7}}[(1-p)|1100\rangle$$
$$+ p|0011\rangle + \sqrt{p(1-p)}|1001\rangle$$
$$+ \sqrt{p(1-p)}|0110\rangle]. \qquad (11)$$

Figure 2 shows the entanglement for different p obtained from full quantum state tomography. The entanglement between S_1 and S_2 (red squares) decays monotonically until
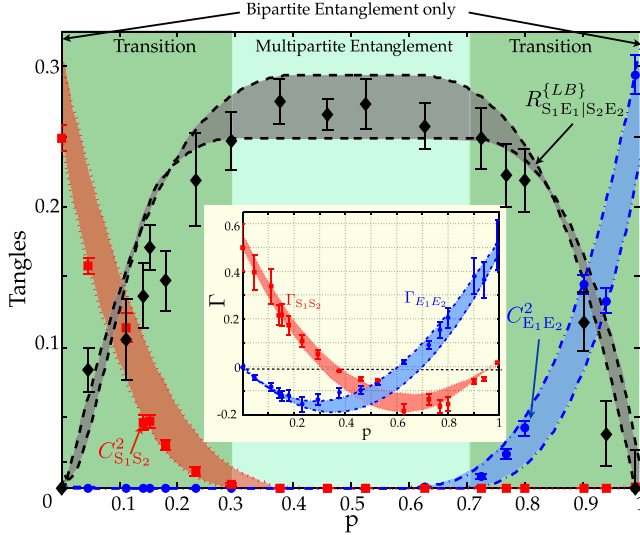
FIG. 2 (color online). Experimental entanglements versus p, the evolution parameter. $C^2_{S_1 S_2}$ is plotted in red squares and $C^2_{E_1 E_2}$ in blue circles. Black diamonds represent the residual entanglement of Eq. (6), in the lower-bound approximation. The areas are theoretical predictions (see the text). The inset shows the evolution of Γ [see Eq. (2)].

it disappears (ESD) at $p_{ESD} = 0.34 \pm 0.04$. This value is close to the theoretical one $|\alpha/\beta| = \sqrt{1/6} \simeq 0.4$. The discrepancy can be attributed to the fact that p_{ESD} is $|\alpha/\beta|$ for pure states, while the experimental states are slightly mixed. At $p_{ESB} = 0.67 \pm 0.05$, bipartite entanglement reappears, but now swapped to the environment qubits [5]. This result is close to the theoretical value $1 - |\alpha/\beta| \simeq 0.6$ for pure states. The inset of Fig. 2 shows the evolution of Γ [see Eq. (2)]. Note that $\Gamma_{E_1 E_2}$ (blue circles) is negative for $p < p_{ESB}$, thus corroborating that the entanglement between E_1 and E_2 is null before the ESB. Similarly, after the ESD, $\Gamma_{S_1 S_2}$ also becomes negative. The values of $C^2_{S_1 E_2}$ and $C^2_{S_2 E_1}$ are nearly 0 during the evolution and are not shown. Black diamonds indicate the residual entanglement in Eq. (6), with $C^2_{S_1 E_1 | S_2 E_2}$ calculated in the lower-bound approximation [8,16]:

$$C^2_{S_1 E_1 | S_2 E_2} \geq [C^{\{LB\}}_{S_1 E_1 | S_2 E_2}]^2 = 2[\mathrm{tr}(\rho) - \mathrm{tr}(\rho_{S_1 E_1})], \quad (12)$$

with ρ the complete density matrix. The theoretical predictions for the experimental results are given by the curved shaded regions in Fig. 2. The curves that limit the shaded regions from below correspond to the theoretical evolution [Eq. (10)] of the initial experimental state found at $p = 0$, for higher values of p. The curves that limit from above correspond to theoretical evolution of the initial state obtained by evolving back the experimental final state found at $p = 1$, for lower values of p. In the absence of experimental imperfections, these curves would coincide. Therefore, the shaded areas represent regions where the

experimental points can be considered compatible with the theory.

For $p_{ESD} \leq p \leq p_{ESB}$, no qubit-qubit entanglement contributing to Eq. (6) is observed, and in agreement with the theoretical result in Ref. [17], the residual entanglement $R_{S_1 E_1 | S_2 E_2}$ reaches its maximum value. Thus, the entanglement changes its nature along the evolution. At $p = 0$, it is exclusively bipartite between S_1 and S_2. In the transition interval (dark green region) $p \in (0, p_{ESD})$, bipartite and multipartite entanglement coexist. Between p_{ESD} and p_{ESB} (light green region), the entanglement is entirely multipartite, and after another transition interval ($p \in (p_{ESB}, 1]$), the evolution ends up with the initial bipartite entanglement, but now involving E_1 and E_2.

Further decomposition of the multipartite entanglement.—An explicit decomposition of $R_{S_1 E_1 | S_2 E_2}$ in terms of well-identified multipartite entanglements is needed to provide detailed information regarding the distribution of entanglement. We first use Eqs. (7) (applied to $i = S_1, E_1$) and (6) to write

$$\mathcal{R}_{S_1 E_1} = \mathcal{E}_0^2 + 2C^2_{S_1 E_1} - (C^2_{S_1 | S_2 E_1 E_2} + C^2_{E_1 | S_1 S_2 E_2}), \quad (13)$$

where we defined $\mathcal{R}_{S_1 E_1} \equiv R_{S_1 E_1 | S_2 E_2} - (R_{S_1} + R_{E_1})$. Since $\mathcal{R}_{S_1 E_1}$ is a linear combination of residual multipartite entanglements, it must be possible to express it in terms of nonbipartite entanglement contributions only. To achieve this, we first use Eq. (5) and observe that $|\Psi(t)\rangle$ can be obtained by applying $U_{S_2 E_2}$ to the intermediate state $U_{S_1 E_1}(t)|\Psi(0)\rangle$. As stated below Eq. (5), $\rho_{S_2 E_2}$ has rank two; hence, at this stage, the problem is that of a three-qubit $[S_1, E_1, \text{and} (S_2 E_2)]$ system in a pure state, and in which only S_1 and E_1 interact. In this case, one multipartite entanglement arises, corresponding to the three-tangle in Eq. (8) with the qubit i being S_1, j being E_1, and k being the effective two-level system $(S_2 E_2)$. We denote this quantity as $\tau_{S_1 E_1 (S_2 E_2)}$.

Because of the invariance of entanglement under local operations, $\tau_{S_1 E_1 (S_2 E_2)}$ remains unaffected when $U_{S_2 E_2}$ acts on $U_{S_1 E_1}(t)|\Psi(0)\rangle$, so the final state $|\Psi(t)\rangle$ has a multipartite entanglement $\tau_{S_1 E_1 (S_2 E_2)}$ whose value is independent of $U_{S_2 E_2}$. On the other hand, according to Eq. (13), $\mathcal{R}_{S_1 E_1}$ depends only on the reduced density matrices $\rho_{S_1 E_1}$, ρ_{S_1}, and ρ_{E_1} and consequently represents a multipartite entanglement that does not depend on $U_{S_2 E_2}$ either. Since $\tau_{S_1 E_1 (S_2 E_2)}$ and $\mathcal{R}_{S_1 E_1}$ are both independent of $U_{S_2 E_2}$, we can compute them, assuming that $U_{S_2 E_2} = \mathbb{I}$. In this case, E_2 remains in its ground state, $(S_1 S_2 E_1)$ remains in a pure state, and thus, $\tau_{S_1 E_1 (S_2 E_2)}$ is given by the three-tangle $\tau_{S_1 S_2 E_1}$ corresponding to the three-qubit state calculated with Eq. (8). As for $\mathcal{R}_{S_1 E_1}$, we notice that with $U_{S_2 E_2} = \mathbb{I}$, we can apply the decomposition (8) to $C^2_{S_1 | S_2 E_1 E_2} = C^2_{S_1 | S_2 E_1}$, to $C^2_{E_1 | S_1 S_2 E_2} = C^2_{E_1 | S_1 S_2}$, and to $\mathcal{E}_0^2 = C^2_{S_1 E_1 | S_2 E_2} = C^2_{S_2 | S_1 E_1}$, thus obtaining $\mathcal{R}_{S_1 E_1} = -\tau_{S_1 S_2 E_1} = -\tau_{S_1 E_1 (S_2 E_2)}$. From the definition of $\mathcal{R}_{S_1 E_1}$, we arrive at

$$R_{S_1 E_1 | S_2 E_2} = R_{S_1} + R_{E_1} - \tau_{S_1 E_1 (S_2 E_2)}. \qquad (14)$$

Decomposition of the R_i allows us to express $R_{S_1 E_1 | S_2 E_2}$ in terms of more explicit multipartite entanglement contributions. This can be accomplished considering that if $\rho_{S_2 E_2}$ is a rank-two matrix, so that the subsystem $(S_2 E_2)$ can be considered as single qubit, and the complete system $S_1 E_1 (S_2 E_2)$ is in a pure state, then we can use Eq. (8) and write

$$C_{i|jkl}^2 = C_{i|j(kl)}^2 = C_{ij}^2 + C_{i(kl)}^2 + \tau_{ij(kl)}$$
$$= C_{ij}^2 + C_{ik}^2 + C_{il}^2 + \tau_{ikl} + \tau_{ij(kl)}, \qquad (15)$$

where in the second line, we used Eq. (1) and denoted with τ_{ikl} the corresponding residual entanglement. The underline distinguishes the reference qubit and stresses the fact that τ_{ikl} is not necessarily invariant under a permutation of indices that involves i, as is τ_{ijk} in Eq. (8). In fact, τ_{ikl} coincides with τ_{ijk} only when ikl is in a pure state. Comparison of Eqs. (7) and (15) leads to

$$R_i = \tau_{ikl} + \tau_{ij(kl)}, \qquad (16)$$

an expression that allows us to compute the tripartite entanglement τ_{ikl} of the mixed state ρ_{ikl} as

$$\tau_{ikl} = C_{i|jkl}^2 - (C_{ij}^2 + C_{ik}^2 + C_{il}^2) - \tau_{ij(kl)}. \qquad (17)$$

Equations (14) and (16) and the analogous equation that results from the latter by substituting $1 \leftrightarrow 2$ lead to

$$R_{S_1 E_1 | S_2 E_2} = \frac{1}{2} [\tau_{S_1 S_2 E_2} + \tau_{S_2 S_1 E_1} + \tau_{E_1 S_2 E_2}$$
$$+ \tau_{E_2 S_1 E_1} + \tau_{S_1 E_1 (S_2 E_2)} + \tau_{S_2 E_2 (S_1 E_1)}]. \qquad (18)$$

We now analyze our experimental data regarding R_i. Direct calculation shows that for the state (11) $\tau_{S_1 E_1 (S_2 E_2)} = \tau_{S_2 E_2 (S_1 E_1)} = 0$ for all p, whence $R_i = \tau_{ikl}$. Figure 3 shows the experimental results for τ_{ikl} of Eq. (17) taking the values of $C_{i|jkl}^2$ in the quasipure approximation [18]. We also compute $\tau_{ij(kl)}$ in the quasipure approximation and verify that $\tau_{ij(kl)} \leq 0.03$ for all $ij(kl)$, so that the experimental $\tau_{ijk} \simeq R_i$. The theoretical predictions, curves (dashed lines) shown in Fig. 3, are calculated for pure states. In this case, we can directly compute the three-tangles in Eq. (17) for the state in Eq. (11) taking different values of p. In addition, for the present interaction between S_i and E_i, it can be shown that $\tau_{S_1 S_2 E_2} = \tau_{S_2 S_1 E_1}$ and $\tau_{E_1 S_2 E_2} = \tau_{E_2 S_1 E_1}$. We can see that, within the error bars, $\tau_{S_1 S_2 E_2}$ (red circles) and $\tau_{S_2 S_1 E_1}$ (black diamonds) coincide, in agreement with these predictions. The same goes for $\tau_{E_1 S_2 E_2}$ (blue squares) and $\tau_{E_2 S_1 E_1}$ (magenta stars). Moreover, in all maxima, the experimental states have smaller τ_{ikl} than those predicted for pure states (dashed lines). This is related to the impurity
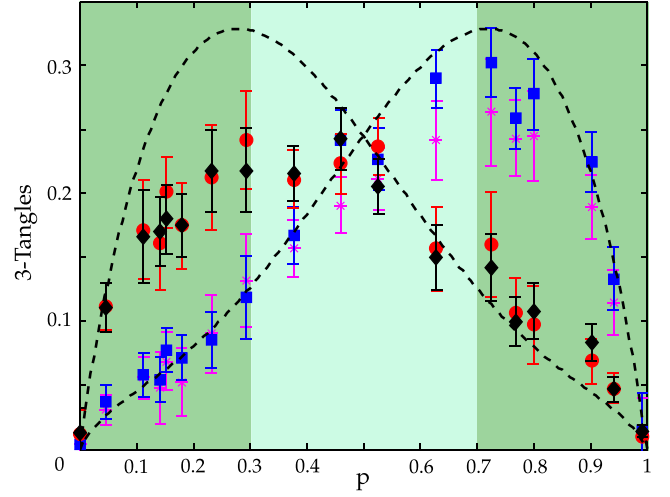

FIG. 3 (color online). Three-tangles τ_{ijk} in the quasipure approximation versus p. Red circles represent $\tau_{S_1 S_2 E_2}$, black diamonds $\tau_{S_2 S_1 E_1}$, blue squares $\tau_{E_1 S_2 E_2}$, and magenta stars $\tau_{E_2 S_1 E_1}$. The dashed lines are a theoretical prediction for pure states.

of the experimental states and to the fact that τ_{ikl} is computed from the experimentally reconstructed states in the quasi-pure approximation, which is a lower bound for this quantity [18]. Notice that $\tau_{S_1 S_2 E_2}$ reaches its maximum nearly at p_{ESD}, and analogously, $\tau_{S_1 S_2 E_2}$ reaches its maximum nearly at p_{ESB}.

Previously, we showed that the evolved state possesses tripartite entanglement in the form τ_{ikl}. The emergence of genuine four-partite entanglement is demonstrated using the fidelities $F_{|\psi\rangle} = \langle \psi | \rho | \psi \rangle$ of an experimental state ρ with respect to a genuine multipartite entangled state $|\psi\rangle$, as witnesses of multipartite entanglement. In particular, ρ is genuinely four-partite entangled if $F_{|\psi\rangle} > \mathcal{O}$, where $\mathcal{O}$ is
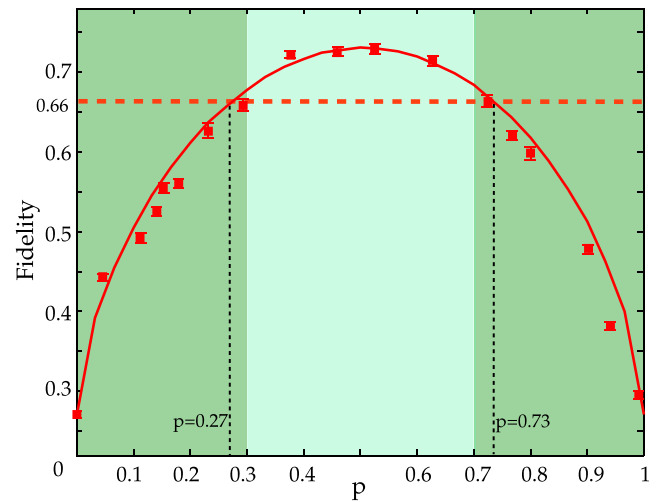

FIG. 4 (color online). Fidelity with respect to the Dicke state $|\mathcal{D}\rangle$ versus p. The line is the theoretical evolution of the experimental initial state.

the maximal overlap between $|\psi\rangle$ and all the biseparable states [19]. We note that the states in Eq. (11) look very similar to the state $|\mathcal{D}\rangle = 1/\sqrt{6}(|0000\rangle + |1111\rangle + |0011\rangle + |1100\rangle + |0110\rangle + |1001\rangle)$, which is a Dicke state with the second and fourth qubits flipped [20]. Moreover, $F_{|\mathcal{D}\rangle} > 2/3$ is sufficient to witness genuine four-partite entanglement [19]. The fidelities $F_{|\mathcal{D}\rangle}$ for our experimental states are shown in Fig. 4. The experimental points (red squares) are in good agreement with the fidelities between $|\mathcal{D}\rangle$ and the theoretical evolution of the initial (experimental) state. Furthermore, in the interval $p \in [0.27, 0.73]$, the fidelities exceed 2/3, demonstrating the presence of genuine four-partite entanglement.

Conclusions.—We presented an experimental investigation of the spread of entanglement from two entangled qubits to their local environments, which is quite challenging for other physical systems, since, in general, the environmental degrees of freedom are inaccessible. We observed the transition of bipartite ↔ multipartite entanglement along the evolution and showed that ESD occurs when the entanglement becomes completely multipartite, whereas ESB occurs when the entanglement ceases to be completely multipartite and gets redistributed in bipartite form. We believe that this is the first experimental demonstration of ESB. We also presented a novel decomposition of the residual entanglement that allowed us to analyze our results in terms of well-identified three- and four-partite entanglement contributions. Furthermore, we used the fidelity as a witness of multipartite entanglement to demonstrate the emergence of a genuine four-partite entangled state during the evolution. Our results represent a significant step towards a deeper understanding of decoherence processes and the distribution of entanglement in multiqubit systems.

*gabo@if.ufrj.br

[1] E. Schrödinger, Naturwissenschaften **23**, 807 (1935); **23**, 823 (1935); **23**, 844 (1935).
[2] W. H. Zurek, Rev. Mod. Phys. **75**, 715 (2003).
[3] T. Yu and J. H. Eberly, Phys. Rev. Lett. **93**, 140404 (2004).
[4] M. P. Almeida, F. de Melo, M. Hor-Meyll, A. Salles, S. P. Walborn, P. H. S. Ribeiro, and L. Davidovich, Science **316**, 579 (2007).
[5] C. E. Lopez, G. Romero, F. Lastra, E. Solano, and J. C. Retamal, Phys. Rev. Lett. **101**, 080503 (2008).
[6] D. M. Greenberger, M. Horne, and A. Zeilinger, Phys. Today **46**, No. 8, 22 (1993).
[7] W. Dür, G. Vidal, and J. I. Cirac, Phys. Rev. A **62**, 062314 (2000).
[8] O. Jiménez-Farías, G. H. Aguilar, A. Valdés-Hernández, P. H. Souto Ribeiro, L. Davidovich, and S. P. Walborn, Phys. Rev. Lett. **109**, 150403 (2012).
[9] G. H. Aguilar, O. Jiménez-Farías, A. Valdés-Hernández, P. H. Souto Ribeiro, L. Davidovich, and S. P. Walborn, Phys. Rev. A **89**, 022339 (2014).
[10] T. J. Osborne and F. Verstraete, Phys. Rev. Lett. **96**, 220503 (2006).
[11] W. K. Wootters, Phys. Rev. Lett. **80**, 2245 (1998).
[12] Y.-K. Bai, M.-Y. Ye, and Z. D. Wang, Phys. Rev. A **80**, 044301 (2009).
[13] V. Coffman, J. Kundu, and W. K. Wootters, Phys. Rev. A **61**, 052306 (2000).
[14] P. G. Kwiat, E. Waks, A. G. White, I. Appelbaum, and P. H. Eberhard, Phys. Rev. A **60**, R773 (1999).
[15] D. F. V. James, P. G. Kwiat, W. J. Munro, and A. G. White, Phys. Rev. A **64**, 052312 (2001).
[16] F. Mintert and A. Buchleitner, Phys. Rev. Lett. **98**, 140505 (2007).
[17] J. G. G. de Oliveira, Jr., J. G. Peixoto de Faria, and M. C. Nemes, Phys. Lett. A **375**, 4255 (2011).
[18] F. Mintert and A. Buchleitner, Phys. Rev. A **72**, 012336 (2005).
[19] W. Wieczorek, C. Schmid, N. Kiesel, R. Pohlner, O. Gühne, and H. Weinfurter, Phys. Rev. Lett. **101**, 010503 (2008).
[20] N. Kiesel, C. Schmid, G. Tóth, E. Solano, and H. Weinfurter, Phys. Rev. Lett. **98**, 063604 (2007).